Design of a Microengineered Electrostatic Quadrupole Lens

Richard R. A. Syms, *Member, IEEE,* Thomas J. Tate, Munir M. Ahmad, and Stephen Taylor, *Member, IEEE*

***Abstract*— The design of a miniature quadrupole lens based on metallized glass electrodes mounted in two anisotropically etched silicon mounts that are separated by precision spacers is described. The analysis of conventional quadrupole lenses is first reviewed. The fabrication process is then described, and the analysis techniques are applied to the new geometry. The potential distribution near the axis is first calculated using a finite difference method. Expansion into solutions of Laplace's equation in cylindrical coordinates is then used to determine the potential distortion introduced by the microengineered mount. Design rules are given for a mount and an electrode radius that achieve minimal distortion.**

***Index Terms*— Mass spectrometer, microengineering, quadrupole lens, residual gas analysis.**

I. Introduction

THE miniaturization of mass spectrometers offers the intriguing prospect of low-cost universal gas detection, because of the likely reduction in the pumped volume and the possibility of high-pressure operation. Due to the rapid development of suitable fabrication techniques, there has recently been an upsurge of interest in the development of microengineered instruments. Typically, mass spectrometers involve three main subsystems: an ion source, an ion filter, and an ion counter. Since these may all be based on several different operating principles, there is scope for a variety of microengineered designs to evolve. Here, we consider filter variants.

A microengineered spectrometer based on a time-of-flight filter has been successfully developed at Johns Hopkins Applied Physics Laboratory [1]–[3]. Spectrometers and spectrographs based on crossed-field Wien filters have also been developed at Rosemount Analytical, Inc., Eden Prairie, MN [4] and Westinghouse, Pittsburgh, PA (now continued by Northrop Grumman) [5]–[7], respectively. However, few attempts have been made to integrate the most popular design of macroscopic instrument, the quadrupole mass spectrometer.

Two very similar forms of miniaturized (but not microengineered) electrostatic quadrupole lens arrays have been demonstrated by Ferran Scientific Inc., San Diego, CA [8], [9] and the Jet Propulsion Laboratory (JPL), Pasadena, CA [10], [11]. A rather different hyperbolic quadrupole lens has also been constructed from metallized, machined Si_3N_4 by the Japan Atomic Energy Research Institute [12]. There is some evidence that a microengineered quadrupole array was fabricated using the LIGA process in a collaboration between JPL and Brookhaven National Laboratory [13]; however, we have been unable to identify any publications that describe its operation. Further JPL-sponsored work involving an ion trap (rather than a simple quadrupole filter) is also continuing at Polychip, Inc., Washington, DC [14].

In our own work, we have attempted to develop miniaturized electrostatic quadrupole lenses using a MEMS approach, based on metallized glass electrodes mounted in two anisotropically etched silicon mounts that are separated by precision spacers [15], [16]. The design has the two key advantages that it is not only self-aligning but also self-compensating for variations in etch selectivity, thus allowing constructional precision to be maintained to the tolerance required. However, it has the disadvantage that the etched Si substrates are extremely close to the electrodes. Given this, it is unclear that a potential distribution of appropriately low distortion will be established in the important axial region.

Crude mass-spectrometer action has already been demonstrated using prototype lenses with 500-μm diameter electrodes [17]. Using an improved mount design, a resolution at 10% peak height of 2.7 u (atomic mass units) at mass 40 was recently obtained using a 30-mm-long lens with similar electrodes, operating at an RF frequency of 6 MHz [18]. This resolution is considerably lower than that achieved in more conventional miniaturized quadrupoles [9], [11], but is now approaching that achieved in microenginered crossed-field devices [5]–[7].

The aim of this paper is to describe the design in more detail, and show that good electrostatic performance can indeed be obtained, provided the geometry of the silicon mount is chosen correctly. The analysis techniques applied to conventional quadrupole lenses are first reviewed in Section II. The microengineered lens is described in Section III; in Section IV, the analysis techniques previously introduced are applied to this geometry, with the overall aim of optimizing the electrostatic performance within the constraints involved. Simple design formulas for the optimum arrangement are then presented in Section V.

Manuscript received April 29, 1998; revised July 17, 1998. The review of this paper was arranged by Editor K. Najafi. This work was supported by the EPSRC through Grant GR/K55868.

R. R. A. Syms, T. J. Tate, and M. M. Ahmad are with the Optical and Semiconductor Devices Section, Department of Electrical and Electronic Engineering, Imperial College, London SW7 2BT U.K. (e-mail: r.syms@ic.ac.uk).

S. Taylor is with the Department of Electrical Engineering and Electronics, Liverpool University, Liverpool L69 3BX, U.K.

Publisher Item Identifier S 0018-9383(98)07836-8.

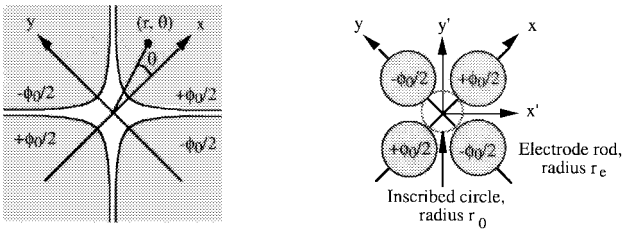

(a) (b)

Fig. 1. (a) Exact and (b) approximate electrostatic quadrupole lens geometries.

II. Design of Conventional Electrostatic Quadrupole Lenses

We begin by considering the design of conventional electrostatic quadrupole lenses. An ideal quadrupole consists of four parallel electrodes with hyperbolic cross-sections, which carry potentials $\pm\phi_0/2$, as shown in Fig. 1(a) [19]–[21]. These electrodes establish a two-dimensional potential variation of the form:

$$\phi(x,y) = \phi_0(x^2 - y^2)/2r_0^2 \tag{1}$$

where r_0 is the radius of the circle touching the equipotentials $\phi = \pm\phi_0/2$. This field will exert forces in the x- and y-directions on an ion moving in the z-direction. The equation of motion due to forces in the x-direction is $md^2x/dt^2 = -e\partial\phi/\partial x = -e\phi_0 x/r_0^2$, where e and m are the charge and mass of the ion. When the time variation of the potential is $\phi_0(t) = U - V\cos(\omega t)$, where $\omega = 2\pi f$ is an angular frequency and U and V are constant potentials, this equation of motion reduces to

$$d^2x/dt^2 + (e/mr_0^2)\{U - V\cos(\omega t)\}x = 0. \tag{2}$$

Using the substitutions $t = 2\zeta/\omega, a = 4eU/(m\omega^2 r_0^2)$ and $q = 2eV/(m\omega^2 r_0^2)$, Equation (2) can then be reduced to the Matthieu equation

$$d^2x/d\zeta^2 + \{a - 2q\cos(2\zeta)\}x = 0. \tag{3}$$

Stable solutions to (3) are only obtained for values of a and q within an approximately triangular region of the q–a plane, and hence for particular combinations of U, V, and m. Because these solutions correspond to bounded ion trajectories, the quadrupole has a mass-dependent filter action. The apex of the stability diagram lies at $a = 0.237, q = 0.706$, so that $a/2q = U/V = 0.168$. If U and V are scanned, maintaining this ratio, the passband tunes through the stability diagrams of different masses, and the lens acts as a mass spectrometer.

Because of the difficulty of machining electrodes with hyperbolic cross-sections, cylindrical rods are generally used, as shown in Fig. 1(b). Experiments have shown that the best approximation to the field of (1) is obtained when their radius r_e is $r_e = 1.148r_0$ [22], [23]. Numerical solution of Laplace's equation has confirmed this result, but the use of a grounded shroud round the electrodes can alter the optimum radius [24].

Now, the number of cycles of the RF field experienced by an ion traveling through the lens is

$$n \approx fL/v = fL\sqrt{\{m/2eV_z\}} \tag{4}$$

where L is the length of the lens, v is the axial ion velocity, and V_z is the axial ion energy in volts. By numerical integration of ion trajectories (see e.g. [25]), it has been shown that the mass resolution depends on n according to

$$m/\Delta m \approx n^2/20 = f^2L^2m/40eV_z. \tag{5}$$

So that the uncertainty in mass is

$$\Delta m \approx 40eV_z/f^2L^2 \approx 3.854 \times 10^9\ V_z/f^2L^2 \tag{6}$$

where Δm is measured in atomic mass units (u). The maximum ac voltage $V_{\max}$ required is then determined by the maximum mass $m_{\max}$ (again, in atomic mass units) as:

$$V_{\max} = m_{\max}q\omega^2 r_0^2/2e = 14.46 \times 10^{-8} m_{\max} f^2 r_0^2 \tag{7}$$

A conventional quadruple might be constructed from 5 mm diameter electrodes (so that $r_0 = 2.177$ mm), with a length of 10 cm. Assuming that $m_{\max} \approx 100$ u, the maximum peak ac voltage required is $V_{\max} \approx 1.1$ kV at 4 MHz. A voltage of this magnitude is typically provided by arranging each electrode pair to act as the capacitative part of an RF resonator. Assuming further that the axial ion energy is held at a minimum of (say) 2 eV, the uncertainty in mass is only $\Delta m \approx 0.05$ u. However, this resolution requires a costly, fragile mount capable of holding the electrodes accurately parallel at the desired separation [25].

By reducing the electrode diameter to 500 μm, it is possible to reduce the maximum ac voltage to around 11 V at a similar frequency. If the electrode length is also reduced by an order of magnitude, the uncertainty in mass exceeds 1 u; however, a resolution of around 1 u may be obtained for $L > 2$ cm. These results suggest that it will be possible to construct a miniaturized instrument of low resolution, given a suitable electrode mounting.

In a conventional quadrupole, the use of cylindrical electrodes and a grounded shroud both result in a distorted potential distribution ϕ', which reduces the performance of the lens. Differences between the ideal and the actual distribution are quantified as follows [22], [24]. The potential ϕ' is first computed near the axis. An expansion ϕ'' of this distribution in terms of a set cylindrical harmonics is then created, so that

$$\phi'(r,\theta) \approx \phi''(r,\theta) = \sum_{m=1}^{\infty} C_m\phi_{cm} + \sum_{n=1}^{\infty} S_n\phi_{sn} \tag{8}$$

where C_m and S_n are constant coefficients and the terms ϕ_{cm} and ϕ_{sn} are given by

$$\phi_{cm} = (r/r_0)^m\cos(m\theta), \quad \phi_{sn} = (r/r_0)^n\sin(n\theta). \tag{9}$$

Equation (9) represent the complete set of two-dimensional solutions to Laplace's equation in cylindrical coordinates, namely $1/r\partial(r\partial\phi/\partial r)/\partial r + 1/r^2\partial^2\phi/\partial r^2 = 0$, that are finite over the range $0 \le r \le r_0$. Symmetry reduces the number of terms allowed in the expansion. For example, when potentials $\pm\phi_0/2$ are applied to cylindrical electrodes that have their centers on the corners of a square, the potential distribution must be antisymmetric about the lines $x = y$ and $x = -y$,

and symmetric about $x = 0$ and $y = 0$. The antisymmetry conditions imply that

$$\phi''(\theta) = -\phi''(\pi/2 - \theta) \quad \text{and} \quad \phi''(\theta) = -\phi''(-\pi/2 - \theta) \tag{10}$$

To satisfy (10), we require $\cos(m\pi/2) = -1$ and $\cos(n\pi/2) = +1$, so m and n can only have the values $m = 2$, 6, 10 $\cdots$ and $n = 4$, 8, 12 $\cdots$. However, the symmetry conditions imply that

$$\phi''(\theta) = \phi''(-\theta) \quad \text{and} \quad \phi''(\theta) = \phi''(\pi - \theta). \tag{11}$$

Equations (11) can be satisfied if $\cos(m\pi) = 1$, i.e., with $m = 2$, 4, 6, $\cdots$, but they cannot be satisfied with any value of n. Thus, if the symmetry and antisymmetry conditions apply simultaneously (as in a conventional quadrupole), the allowed terms are restricted to ϕ_{cm} with $m = 2(2i+1)$. If the symmetry condition is relaxed, extra terms ϕ_{sn} with $n = 4j$ are permitted; this occurs in the case of our microengineered quadrupole, as we shall see in Section IV.

Considering the term ϕ_{c2} in isolation, we can see that this component can be written as

$$\begin{aligned}\phi_{c2} &= (r/r_0)^2 \cos(2\theta) = (r/r_0)^2\{\cos^2(\theta) - \sin^2(\theta)\} \\ &= (x^2 - y^2)/r_0^2.\end{aligned} \tag{12}$$

An ideal hyperbolic potential can be represented by (8) with $C_2 = \phi_0/2$ and all other coefficients zero. Nonzero values of other coefficients therefore correspond to field imperfections, which couple together ion motions in the x- and y-directions. Since the higher order terms diminish rapidly for $r < r_0$, the best approximation to the desired field is obtained by minimizing the coefficients C_6, S_4, and S_8.

The allowed expansion coefficients are chosen to give the best representation of the potential, where 'best' is defined as the least squared error between ϕ' and ϕ'' integrated over the circle $0 \le r \le r_0$. In view of the known field symmetries, the integration need only be made over one quadrant, so the error e that must be minimized is defined by

$$e^2 = \int_{-\pi/4}^{\pi/4} \int_0^{r_0} \left\{ \phi' - \left(\sum_{m=1}^{\infty} C_m \phi_{cm} + \sum_{n=1}^{\infty} S_n \phi_{sn} \right) \right\}^2 r\, dr\, d\theta \tag{13}$$

Denison [24] computed the coefficient values by using numerical data to set up a large number of simultaneous equations, increasing the number until no change was seen in the values of the first few coefficients. However, the orthogonality of the functions ϕ_{cm} and ϕ_{sn} over the integration range suggests that the coefficients may be found unambiguously as follows. At stationary points in e^2, the conditions $\partial e^2/\partial C_m = \partial e^2/\partial S_n = 0$ must hold. Differentiation then allows the coefficients C_m to be found as overlap integrals of the form $C_m = I_{am}/I_{bm}$, where

$$\begin{aligned} I_{am} &= \int_{-\pi/4}^{\pi/4} \int_0^{r_0} \phi' \phi_{cm} r dr d\theta \\ I_{bm} &= \int_{-\pi/4}^{\pi/4} \int_0^{r_0} \phi_{cm}^2 r dr d\theta. \end{aligned} \tag{14}$$

In a similar way, the coefficients S_n are given by $S_n = I_{cn}/I_{dn}$, where

$$\begin{aligned} I_{cn} &= \int_{-\pi/4}^{\pi/4} \int_0^{r_0} \phi' \phi_{sn} r dr d\theta \\ I_{dn} &= \int_{-\pi/4}^{\pi/4} \int_0^{r_0} \phi_{sn}^2 r dr d\theta. \end{aligned} \tag{15}$$

The integral I_{am} can be evaluated numerically. If values of ϕ' are known on a grid of points of spacing Δ parallel to the x'- and y'-directions in Fig. 1(b), I_{am} is given approximately by

$$\begin{aligned} I_{am} = \sum_i \sum_j \phi'(x_i', y_j') \phi_{cm}(x_i', y_j') \Delta^2, \\ x_i', y_j' \text{ within quadrant of circle of radius } r_o. \end{aligned} \tag{16}$$

Calculations of this type are extremely sensitive to the number of grid points and to their position, so the convergence of the integral must be carefully checked. The integral I_{bm}, however, can be found analytically as

$$I_{bm} = r_0^2 \pi / 8(m+1). \tag{17}$$

C_m is then found from the ratio of (16) and (17), and S_n is found in a similar way.

For a conventional quadrupole with cylindrical electrodes, calculations and experiment [22], [23] have shown that C_6 actually vanishes when the electrode radius has the value mentioned earlier $(r_e = 1.148 r_0)$, explaining the widespread adoption of this design rule. When the lens is surrounded by a cylindrical grounded shroud, Denison found that the optimum value of r_e is increased, but not significantly. However, the precision quoted (four decimal places) was surprising given the nature of the numerical calculation [24].

III. Construction of a Silicon-Based Microengineered Electrostatic Quadrupole Lens

We now consider the construction of our microengineered quadrupole lens. In this case, the four cylindrical electrodes are mounted in pairs on two Si substrates, that are held apart by two cylindrical spacers as shown in Fig. 2 [15]–[18]. V-shaped alignment grooves formed by anisotropic etching [26], [27] are used as kinematic mounts for both the electrodes and the spacers. This mounting method is similar to that used to hold single-mode optical fibers in ribbon fiber connectors [28]–[30]; in each case, positioning accuracy is achieved by the

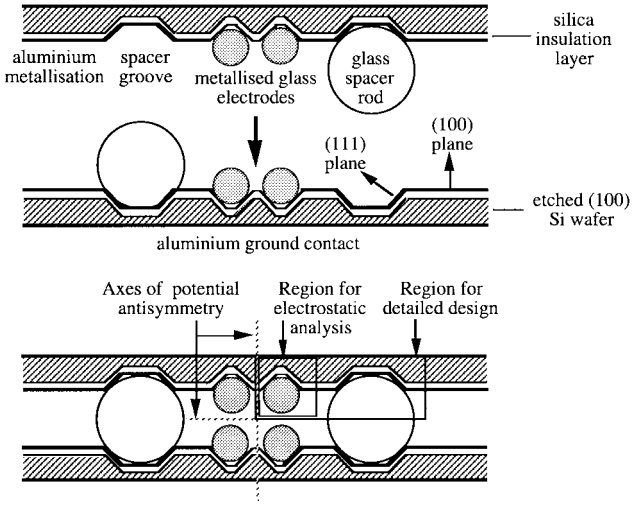

Fig. 2. Self-aligning microengineered electrostatic quadrupole lens assembly.

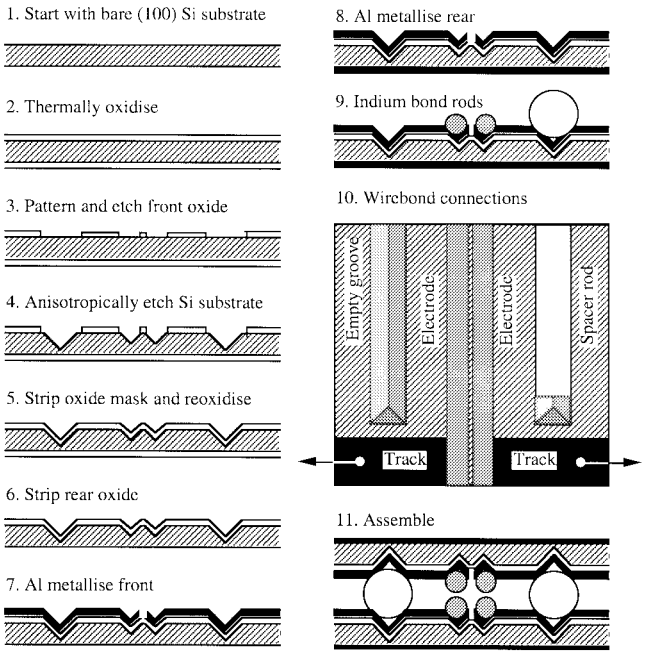

Fig. 3. Process sequence for fabrication of microengineered electrostatic quadrupole lenses.

use of lithography followed by etching along crystal planes. Here, assembly of the two halves of the lens is also naturally self-aligning.

A simple batch fabrication process has been developed for prototype lenses, based on vacuum compatible materials. A process flowchart is shown in Fig. 3, and the most important features of the design are shown in the enlarged views of Fig. 4(a)–(c). The dimensions depend on the desired electrode diameter and substrate separation, as will be discussed in Sections IV and V. Anticipating later results, we shall assume an electrode radius of $r_e = 250\,\mu$m (corresponding to $r_0 = 217.8\,\mu$m), an in-plane electrode center-to-center separation of $s_e = 661.5\,\mu$m, and a spacer radius of $r_s = 822.9\,\mu$m [Fig. 4(a)].

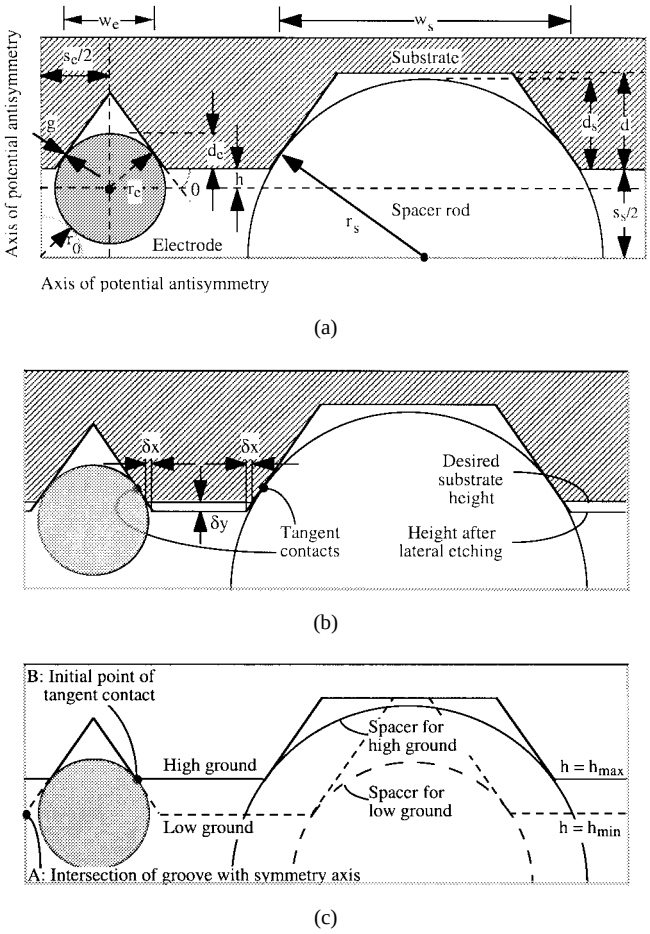

Fig. 4. Geometry of the microengineered electrostatic quadrupole lens, illustrating (a) main design parameters, (b) effect of lateral etching in the self-compensating design, and (c) range of possible ground plane positions.

In our process, 4-in diameter (100) orientated p-type silicon wafers are first thermally oxidized, to a thickness of 1.5 μm (Step 2 in Fig. 3). The front side oxide layer is then patterned and etched in buffered HF to form a surface mask for the anisotropic etch (Step 3). During this step, the back side oxide is protected; because of the deep etching used later, small flaws in the surface mask formed at this stage can cause catastrophic defects. The groove widths required to seat the two types of rod are different. For the parameters above, the electrode and spacer groove widths are $w_e = 408.2\,\mu$m and $w_s = 1343.8\,\mu$m, respectively [Fig. 4(a)].

The silicon is then anisotropically etched at 112 °C in a mixture of ethylene diamine, pyrocatechol and water (EDP) to expose the (111) crystal planes (Step 4 in Fig. 3). These planes lie at an angle of $\theta = \cos^{-1}(I/\sqrt{3}) = 54.74°$ to the wafer surface [26], [27] [Fig. 4(a)]. Due to the difference in size between the two types of rod, the electrode grooves are fully formed, while the spacer grooves are truncated. The minimum groove depths needed to seat the electrode and spacer rods are d_e and d_s, respectively. The etch depth d is chosen to allow clearance for the spacer, so that $d > d_s$. For the parameters above, $d_s = 347.8\,\mu$m, and wafer thicknesses of $\approx 500\,\mu$m are needed to retain sufficient mechanical strength after etching.

In anisotropic etching, the (111) planes are always attacked, albeit at a slower rate than the (100) planes. The etch selectivity s is defined as $s = R_{100}/R_{111}$, where R_{100} and R_{111} are the etch rates of the two planes. For fresh EDP, the selectivity is normally ≈ 35; however, it can be considerably less in old solutions. When etching to a depth of $\approx$350 μm, we might therefore expect to widen the grooves considerably. In order to minimize any subsequent rod misalignment, a design that is not only self-aligning but also self-compensating was adopted.

Fig. 4(b) illustrates the self-compensating design. Here, the electrode and the spacer rod *both form tangent plane contacts with the substrate*. Even though the initial groove width is very different in each case, the effect of lateral etching will then be to widen both grooves on each side by an identical amount $\delta x = d/\{s\sin(\theta)\}$. Individually, the result is to seat each rod deeper in the substrate. However, the *combined* effect is merely to lower the substrate, by an amount $\delta y = \delta x \tan(\theta)$, without altering the relative positions of the electrode and the spacer. The use of double tangent-plane V-groove mounting therefore compensates for finite etch selectivity, and also for variations in selectivity from substrate to substrate. A similar design was previously developed for a miniaturized optical breadboard system [31].

After etching, the oxide mask is removed using BHF, and the wafer is reoxidized to form an insulating layer (Step 5 in Fig. 3). Since the maximum voltage between each electrode and ground is $(V_{\max} + U_{\max})/2 \approx 6.4$ V, an oxide thickness of 1.5 μm results in a field of $\approx 4 \times 10^6$ V/m, well below the breakdown field of thermal silica. The insulation may be removed between the electrodes, to prevent charging. The back side oxide layer is then removed, to allow electrical contact to the substrate (Step 6). Because of the surface topography, the front side contact tracks cannot be defined by lithography; instead, they are formed by shadow-masked evaporation of Al (Step 7). Given the large size of the grooves, alignment tolerances of $\approx 10\,\mu$m are sufficient for this step. A further Al layer is deposited on the rear as a ground connection (Step 8). The wafer is then sawn into dies $\approx$ 7 mm wide.

Each substrate carries two electrodes and one spacer. Both types of rod are formed from borosilicate glass drawn to the required dimension to 1% tolerance. The electrodes are metallized by sputter-coating with 300-Å Cr metal followed by 2000-Å Au, and bonded to the substrate using indium (mpt 156.6 °C). Bonding is carried out under pressure at 180 °C, using an inert atmosphere to prevent degradation of the metal coatings (Step 9). To avoid damage to the connection tracks during assembly, the spacers are cut shorter than the electrodes, and are mounted in grooves that are blind at one end, so that the tracks lie on a flat surface. The substrates are then attached to mounts with appropriate electrical connections (Step 10).

Completed lenses are constructed by placing two dies together under pressure, so that each spacer mates with a groove on the other substrate (Step 11). All degrees of freedom except axial motion are then eliminated. Axial motion could also be removed by using spherical spacers in a Kelvin mount, or by using two orthogonal cylindrical rods.

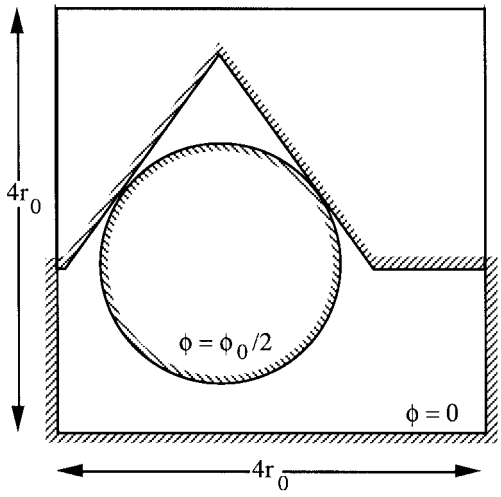

Fig. 5. Boundary potentials assumed for simulation of the microengineered quadrupole lens.

IV. Analysis of the Silicon-Based Microengineered Electrostatic Quadrupole Lens

The electrode mounting method used in our microengineered electrostatic quadrupole involves bringing an etched, grounded substrate close to the axial region in which it is desired to establish the hyperbolic potential distribution. It is therefore important to investigate the effect of the substrate, and to choose the design parameters to minimize any distortion of the potential. In this section, we apply the analysis techniques introduced in Section II to the particular geometry of our microengineered mount.

We first establish the range of adjustable parameters. Fig. 4(c) shows another enlarged view of the mount. Here, the choice of rod radius r_e fixes the position of the electrode center. It is assumed that the electrode is separated from the mount by a narrow gap $g \approx 1.5\,\mu$m, which will in practice be a layer of silica. The value of g makes little difference; however, once it is known, the positions of the crystal planes mounting the electrode are fixed. The only free parameter is then the height h of the substrate above the electrode centerline. Theoretically, its minimum value is found from the intersection of the electrode groove wall with the left-hand axis of symmetry (point A). However, a finite land is required between the two electrode grooves in a real fabrication process. Assuming a minimum value of $h_{\min} = 0$ yields a range that starts close to point A, but allows a suitable land width. The maximum $h_{\max}$ is found as the value at which tangent contact between the electrode and the substrate is just lost (point B).

The dashed lines in Fig. 4(c) therefore show the substrate and spacer rod geometry used when the ground plane is at its lowest possible position, while the full lines show the geometries required when the ground is at its highest possible position. Clearly, a larger spacer is needed to hold the ground plane further from the axis.

To carry out the simulations, we have followed Denison [24] and used the Liebmann method to solve Laplace's equation for the geometry of Fig. 5. Here the electrode potential has been

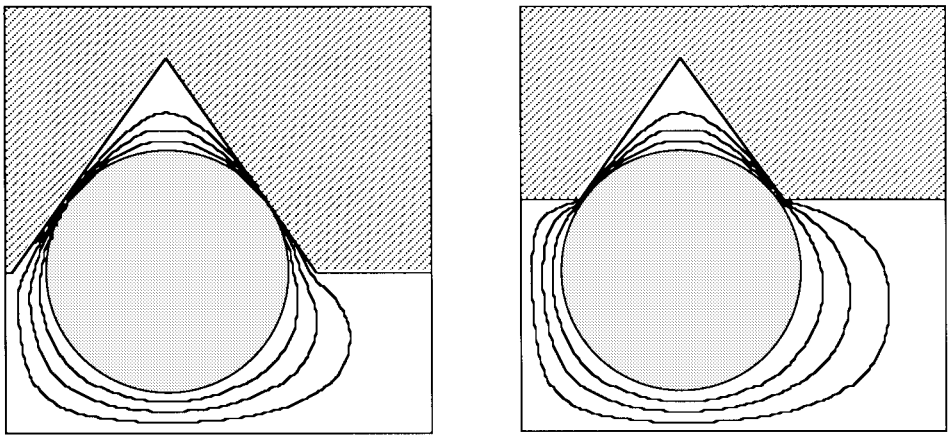

(a) (b)

Fig. 6. Potential variations obtained by numerical solution of Laplace's equation, with the ground plane at (a) its lowest and (b) its highest position. Contours are equally spaced.

fixed at $\phi = \phi_0/2$, and the substrate and axes of potential antisymmetry are assumed to be at $\phi = 0$. An additional boundary (also with $\phi = 0$) has been introduced on the right to limit the range of calculation; provided it is far enough from the axis, this makes little difference to the results.

All calculations were performed on a Sun UltraSparc 1 workstation. After careful investigation of the convergence of the initial potential field calculation, 35 000 iterations were used on a 1800 × 1800 grid of points, with the successive over-relaxation parameter set to 1.7. To improve the convergence of the overlap integrals used to determine the expansion coefficients, further linear interpolation was then used to double the number of potential values in each of the x- and y-directions.

Fig. 6 shows equally-spaced equipotentials obtained with $r_e = 1.148r_0$, for two different values of h, namely $h = 0$ (6a) and $h = h_{\max}$ (6b). The former geometry was used for the prototype lens described in [16], and the latter for the improved device in [18]. In each case, the effect of the etched substrate is to introduce field asymmetry near the left of the figure, because the equipotentials are constrained to pass between the electrode and the substrate at their closest points of approach. However, the asymmetry is greatly reduced in Fig. 6(b), where the substrate is placed further from the axis. It is considered that this feature is responsible for the performance improvement observed in [18].

The variations of the coefficients of the lowest order terms ϕ_{sn} and ϕ_{cm} with h were also computed, again for $r_e = 1.148r_0$. Fig. 7 shows the variation of S_4, S_8, S_{12}, and S_{16} (which describe asymmetric distortions). For the largest coefficients (S_4 and S_8), their values diminish by two orders of magnitude between $h = 0$ and $h = h_{\max}$, showing clearly that optimum performance is obtained when the substrate is as far from the axis as possible. The coefficients C_6 and C_{10} (symmetric distortions) also reduce as h increases, but only slightly.

In fact, the value of the coefficient describing the most important symmetric field distortion (C_6) is more strongly dependent on the electrode radius. Fig. 8 shows the variation

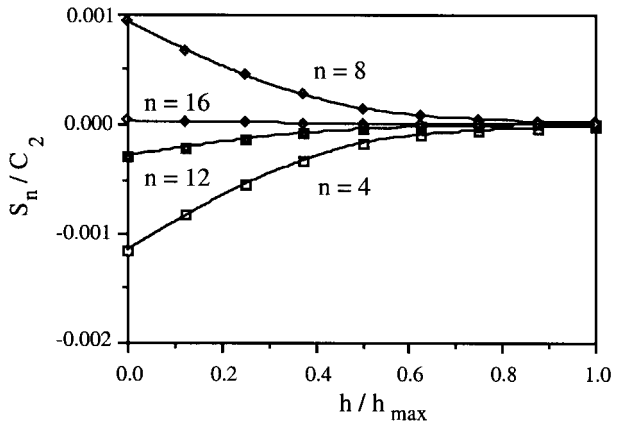

Fig. 7. Variation of the coefficients of the first few low order asymmetric functions ϕ_{sn} with ground plane height h.

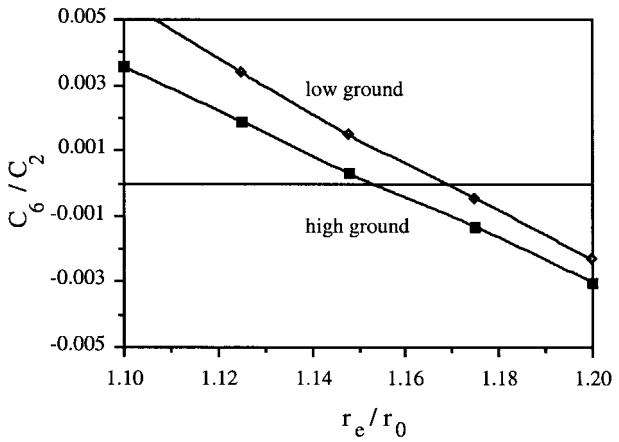

Fig. 8. Variation of the coefficient of the function ϕ_{c6} with electrode radius r_e, for lenses with the ground plane sited at (top) its lowest and (bottom) its highest position.

of C_6 with r_e for microengineered lenses with $h = 0$ (low ground), and $h = h_{\max}$ (high ground). In each case, the variation is quasilinear, passing through zero at an optimum value

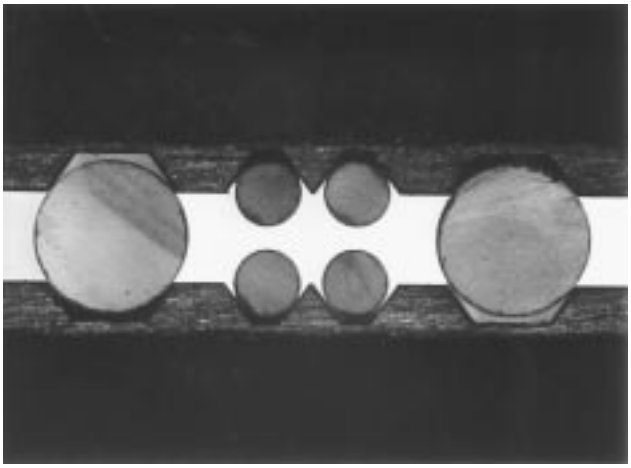

(a)

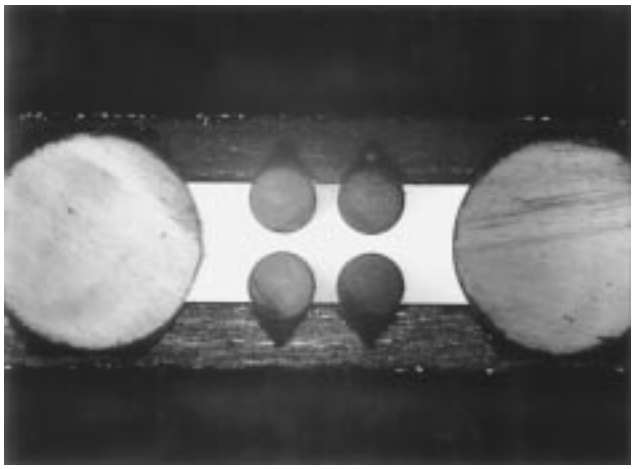

(b)

Fig. 9. Optical microscope photographs of the cross-sections of microengineered quadrupole lenses fabricated with the ground plane at (a) its lowest and (b) its highest position.

of rod radius. The results are therefore qualitatively similar to those obtained by Denison [24]. For lenses with high ground planes, the optimum radius is $r_e \approx 1.151 r_0$, a difference of $\approx$ 0.3% from the conventional value. However, for lenses with low ground planes, this radius is significantly larger. These results indicate that the conventional optimization process can be used for microengineered quadrupoles, and leads to similar design rules.

V. Optimum Design of the Silicon-Based Microengineered Electrostic Quadrupole Lens

Based on arguments advanced in Section IV, the optimum mount design is as shown by the full line in Fig. 4(c). Here, the groove widths are chosen so that the electrodes just form tangent contacts to the etched crystal planes, placing the substrate as far as possible from the axis. Once this has been done, the distance between substrates in an assembled lens is fixed. To minimize the spacer diameter (and hence, to restrict the maximum etch depth needed), the spacer groove widths should then also be chosen so that tangent contacts are just achieved.

Mask design parameters are then calculated as follows. For a particular electrode rod radius r_e, the radius r_0 is first evaluated as described earlier. The in-plane center-to center separation s_e of the electrodes, the radius r_s of the spacer rods, the substrate separation s_s, and the widths w_e and w_s and the minimum depths d_e and d_s of the electrode and spacer grooves are then calculated using (18); these are obtained from Fig. 4 by simple geometry, assuming that cos $(\theta) = \sqrt{(1/3)}$ and sin $(\theta) = \sqrt{(2/3)}$.

$$\begin{aligned} s_e &= \{r_0 + r_e\}\sqrt{2} \quad w_e = 2r_e\sqrt{(2/3)} \\ d_e &= r_e\{1 - 1\sqrt{3}\} \quad r_s = r_e + \{r_0 + r_e\}\sqrt{(3/2)} \\ w_s &= 2r_s\sqrt{(2/3)} \quad d_s = r_s\{1 - 1\sqrt{3}\} \quad s_s = 2r_s/\sqrt{3}. \end{aligned} \tag{18}$$

These equations can be used to find the parameter values previously given in Section III for a lens with 500-μm diameter electrodes. Many lenses of this type have now been fabricated; Fig. 9(a) shows a lens with the ground plane in its lowest possible position (after [16]), and Fig. 9(b) a similar view with the ground in its highest position (after [18]). In each case, the electrodes have their centers on a square as required. However, the increase in spacer rod size needed for the larger substrate separation may clearly be seen.

VI. Conclusions

In this paper, the design of a miniature electrostatic quadrupole lens fabricated using silicon microengineering methods has been described. Electrostatic field calculations have shown that the potential distortion due to the proximity of the grounded substrate used to mount the electrodes can largely be eliminated, in a geometry that retains the two important principles of self-alignment and self-compensation, and that optimization of the electrode radius can follow a procedure similar to that used for conventional quadrupole lenses.

For optimum performance, the design parameters should be chosen so that tangent plane contacts are just achieved between the electrodes and the substrate, and also between the spacer rods and the substrate. Based on this analysis, improved prototypes have been fabricated. Directions of future work currently include improvement in constructional quality, elimination of trace magnetic materials (e.g. Cr), and the development of a complete breadboard quadrupole mass spectrometer system through the addition of a self-aligned microengineered ion source and detector.

Acknowledgment

The authors are grateful to EPSRC and to A. McClure, whose work with early calculations is also gratefully acknowledged.

References

[1] W. A. Bryden, R. C. Benson, S. A. Ecelberger, T. E. Phillips, R. J. Cotter, and C. Fenselau, "The tiny TOF mass spectrometer for chemical and biological sensing," *Johns Hopkins APL Tech. Dig.*, vol. 16, pp. 296–310, 1995.

[2] W. A. Bryden, R. C. Benson, S. A. Ecelberger, T. E. Phillips, T. Cornish, and R. J. Cotter, "Tiny-TOF-MALDI mass spectrometry for particulate drug and explosives detection," *Proc. SPIE*, vol. 2511, pp. 153–164, 1995.
[3] W. A. Bryden, R. C. Benson, H. W. Ko, and M. Donlon, "Universal agent sensor for counterproliferation applications," *Johns Hopkins APL Dig.*, vol. 18, pp. 302–308, 1997.
[4] F. C. Sittler, "Micromachined mass spectrometer," U.S. Patent 5 401 963, 1995.
[5] C. B. Freidhoff, R. M. Young, and S. Sriram, "Solid state micromachined mass spectrograph universal gas detection sensor," U.S. Patent 386 115, 1995.
[6] H. Nathanson, I. Liberman, and C. Freidhoff, "Novel functionality using microgaseous devices," in *Proc. MEMS '95*, Amsterdam, The Netherlands, 1995, pp. 72–76.
[7] C. Freidhoff, "Mass spectrograph on a chip," in *Proc. 1997 IEEE Aerospace Conf.*, Aspen, CO, vol. 3, p. 32, Feb. 1–8, 1997.
[8] R. J. Ferran, "Residual gas sensor utilizing a miniature quadrupole array," U.S. Patent 5 401 962, 1995.
[9] R. J. Ferran and S. Boumsellek, "High-pressure effects in miniature arrays of quadrupole analyzers for residual gas analysis from 10^{-9} to 10^{-2} torr," *J. Vac. Sci. Technol. A*, vol. 14, pp. 1258–1265, 1996.
[10] A. Chutjian, M. H. Hecht, and O. J. Orient, "Miniature quadrupole mass spectrometer array," U.S. Patent 5 719 393, 1996.
[11] O. J. Orient, A. Chutjian, and V. Garkanian, "Miniature, high-resolution, quadrupole mass-spectrometer array," *Rev. Sci. Instrum.*, vol. 68, pp. 1393–1397, 1997.
[12] S. Hiroki, T. Abe, Y. Murakami, Y. Takano, M. Higuchi, and M. Miyake, "Development of a QMS with a ceramic single-piece quadrupole," *Vacuum*, vol. 44, pp. 71–74, 1993.
[13] C. Milne, "LIGA fabricated quadrupolar mass spectrometer array," [Online]. Available at www.nsls.bnl.gov/BeamRD/Chris/jpl02.jpg.
[14] D. B. Salzman, "Mass spectrometer using quadrupolar axialization," NASA Small Business Innovation Research Program Proposal, 13.01-8965, 1995.
[15] S. Taylor, R. R. A. Syms, H. A. Dorey, and T. J. Tate, "Improvements in and relating to quadrupole mass spectrometers," British Patent 9506972.0, 1995.
[16] R. R. A. Syms, T. J. Tate, M. A. Ahmad, and S. Taylor, "Fabrication of a microengineered quadrupole electrostatic lens," *Electron. Lett.*, vol. 32, pp. 2094–2095, 1996.
[17] S. Taylor, J. J. Tunstall, R. R. A. Syms, T. J. Tate, and M. M. Ahmad, "Initial results for a quadrupole mass spectrometer with a silicon micromachined mass filter," *Electron. Lett.*, vol. 34, pp. 546–547, 1998.
[18] S. Taylor, J. J. Tunstall, J. H. Kleck, R. Tindall, P. Julian, J. Batey, R. R. A. Syms, T. J. Tate, and M. M. Ahmad, "Performance improvements for a miniature quadrupole with a micromachined mass filter," in *Proc. 14th Int. Vacuum Congr.*, (IVC-14), Birmingham, U.K., Aug. 31–Sept. 4, 1998.
[19] W. Paul, "Electromagnetic traps for charged and neutral particles," *Rev. Mod. Phys.*, vol. 62, pp. 531–540, 1990.
[20] P. H. Dawson, *Quadrupole Mass Spectrometry and Its Applications*. Amsterdam, The Netherlands: Elsevier, 1976.
[21] J. H. Batey, "Quadrupole gas analyzers," *Vacuum*, vol. 37, pp. 659–668, 1987.
[22] W. C. Elmore and M. W. Garrett, "Measurement of two-dimensional fields. Part I: Theory," *Rev. Sci. Instrum.*, vol. 25, pp. 480–485, 1954.
[23] I. E. Dayton, F. C. Shoemaker, and R. F. Mozley, "The measurement of two-dimensional fields. Part II: Study of a quadrupole magnet," *Rev. Sci. Instrum.*, vol. 25, pp. 485–489, 1954.
[24] D. R. Denison, "Operating parameters of a quadrupole in a grounded cylindrical housing," *J. Vac. Sci. Technol.*, vol. 8, pp. 266–269, 1971.
[25] W. E. Austin, A. E. Holme, and J. H. Leck, "The mass filter: Design and performance," in *Quadrupole Mass Spectrometry and Its Applications*. Amsterdam, The Netherlands: Elsevier, 1976, ch. 6.
[26] D. B. Lee, "Anisotropic etching of silicon," *J. Appl. Phys.*, vol. 40, pp. 4569–4574, 1969.
[27] K. E. Bean, "Anisotropic etching of silicon," *IEEE Trans. Electron Devices*, vol. ED-25, pp. 1185–1193, 1978.
[28] C. M. Schroeder, "Accurate silicon spacer chips for an optical fiber cable connector," *Bell. Syst. Tech. J.*, vol. 57, pp. 91–97, 1977.
[29] Y. Fujii, J. Minowa, and N. Suzuki, "Demountable multiple connector with precise V-grooved silicon," *Electron. Lett.*, vol. 15, pp. 424–425, 1979.
[30] P. C. Chang, S. Sriram, and A. C. Wey, "Multiple fiber interconnect using silicon V-grooves," *Proc. SPIE*, vol. 836, pp. 311–318, 1987.
[31] A. S. Holmes and R. R. A. Syms, "Self-aligning guided wave breadboard system for delay line signal processing," in *Proc. 7th Int. Conf. on Fiber Optics Optoelectronics*, London, U.K., Apr. 25–27, 1989, pp. 3.4–3.9.

Richard R. A. Syms (M'98) was born in Norfolk, VA, in 1958. He received the B.A. degree in engineering science in 1979, and the D.Phil. degree on "volume holographic optical elements" in 1982, both from Worcester College, Oxford, U.K.

He has been Head of the Optical and Semiconductor Devices Section in the Department of Electrical and Electronic Engineering, Imperial College London, since 1992 and Professor of Microsystems Technology since 1996. He has published approximately 70 papers and two books on holography, integrated optics and microengineering. His interests are silica-on-silicon integrated optics based on sol-gel glasses, and silicon-based MEMS. Current MEMS projects include self-assembling 3-D structures, electrostatic and piezoelectric actuators, and microanalytical systems such as a mass spectrometer.

Thomas J. Tate received the Ph.D. degree in physics from City of London Polytechnic, London, U.K., in 1984.

He has since worked in the Department of Electrical and Electronic Engineering, Imperial College London, where he is currently Facilities Manager in the Optical and Semiconductor Devices Section. His research interests include surface modification by ion and electron irradiation (semiconductors, superconductors, mechanical systems, and optics), and vacuum processing of materials. A recent shift of area has been toward microengineering and patterning of materials.

Munir M. Ahmad received the Ph.D. degree in chemistry on the "synthesis, electrical and magnetic properties of organic semiconductors."

Since then he has worked on the design, synthesis and application of electroactive and speciality polymers. He joined the Optical and Semiconductor Devices Section, Department of Electrical and Electronic Engineering, Imperial College London, London, U.K., as a Research Associate in 1993, and has worked on a number of projects related to microengineering and materials for optical devices.

Dr. Ahmad is a Chartered Chemist and a professional member of the Royal Society of Chemistry.

Stephen Taylor (M'96) was born in Liverpool, U.K., in 1956. He received the B.Sc.(Eng) degree in electrical engineering and electronics from Imperial College of Science and Technology, London, U.K., in 1978, and the M.Eng. and Ph.D. degrees from the University of Liverpool in 1983 and 1988, respectively.

He was appointed to a lectureship in the Department of Electrical Engineering and Electronics, Liverpool University, in 1987, becoming Senior Lecturer in 1996.His current research interests include vacuum microelectronics, ion and plasma physics and hot carrier reliability of MOS devices.

Dr. Taylor was a member of the Programme Committee of the IEEE Semiconductor Interface Specialists conference (SISC) from 1995 to 1997.